Available online at www.sciencedirect.com
SCIENCE DIRECT®
International Journal of Heat and Mass Transfer 48 (2005) 3544–3559
International Journal of HEAT and MASS TRANSFER
www.elsevier.com/locate/ijhmt

Thermal and flow behavior of ice slurries in a vertical rectangular channel—Part II. Forced convective melting heat transfer

E. Stamatiou, M. Kawaji *

Department of Chemical Engineering & Applied Chemistry, University of Toronto, 200 College Street, Toronto, Ontario, Canada M5S 3E5

Received 19 February 2004; received in revised form 24 March 2005
Available online 26 May 2005

Abstract

The convective heat transfer characteristics of ice slurries flowing vertically upward in a rectangular channel have been experimentally investigated. At steady state, the local heat transfer coefficients were obtained during convective melting, and the effects of ice fraction, Reynolds number and wall heat flux were determined. To gain more insights into the flow properties, local measurements of the axial mixture velocity, temperature and ice fraction distributions were also made near a heated wall. Four main factors were shown to enhance the convective heat transfer coefficient of ice slurries relative to single-phase flow: (1) the ice fraction, (2) thermally and/or hydrodynamically developing flow conditions, (3) mixed-convection and (4) non-Newtonian effects experienced at $Re < 4000$. Two new and simple heat transfer correlations are also proposed for the practical design of compact heat exchangers involving phase change ice slurries.

Keywords: Ice slurry; Thermal-hydraulics; Compact heat exchangers; Convective heat transfer; Phase change; Non-Newtonian; Mixed-convection

1. Introduction

Forced convective melting of ice slurries in heat exchanger systems has recently been the subject of intense research as ice slurries are environmentally friendly and can be regarded as natural secondary refrigerants for use in refrigeration and air-conditioning applications [1]. The use of ice slurries in heat exchanger systems may also improve the heat transfer performance compared to chilled water, and allow smaller and more compact heat exchangers to be used.

The optimum design of compact heat exchangers for ice slurry use with a large heat transfer area to volume ratio, reduced weight and capital cost, requires good knowledge of the convective heat transfer characteristics accompanied by phase change, which cannot be readily deduced from chilled water data.

Previous investigations dealing with the melting flow and heat transfer properties of ice slurries in tubular and plate heat exchangers have been recently reviewed and discussed by Ayel et al. [2] and Bellas et al. [3]. Other

* Corresponding author. Tel.: +1 416 978 3064; fax: +1 416 978 8605.
E-mail address: kawaji@ecf.utoronto.ca (M. Kawaji).

0017-9310/$ - see front matter © 2005 Elsevier Ltd. All rights reserved.
doi:10.1016/j.ijheatmasstransfer.2005.03.019

Nomenclature

A	area, m^2
C	concentration, %
C_p	heat capacity, J kg^{-1} K^{-1}
D_h	hydraulic diameter, m
g	gravitational constant (=9.81 m/s^2)
Gr	Grashof number ($= g\beta q''_w H^4/\nu^2 k$)
Gz	Graetz number ($=RePrD_h/x$)
H	channel gap, m
h	heat transfer coefficient, W m^{-2} K^{-1}
k	thermal conductivity, W m^{-1} K^{-1}
L	length, m
n	power law index
Nu	Nusselt number
Pr	Prandtl number
Q	volumetric flow rate, m^3 s^{-1}
q''	heat flux, W/m^2
Re	Reynolds number
T	temperature, K
u	axial velocity, m/s
$\langle u \rangle$	volumetric average axial velocity, m/s
V	integrated average axial velocity, m/s
W	channel width, m
x	axial distance from the inlet of heated section, m
x^+	dimensionless distance ($=x/D_h$)
X_s	mass ice fraction, %
y	transverse distance from a heated surface, m
y'	transverse distance from channel axis, m
z	lateral distance, m

Greek symbols

α^*	channel aspect ratio ($=H/W$)
β	volumetric thermal expansion coefficient, K^{-1}
δ_t	"ice free" boundary layer thickness, mm
μ	kinematic viscosity, Pa s
ρ	density, kg m^{-3}
Φ	volumetric ice or solid fraction, %

Subscripts

a	additive
b	brine
c	cross sectional
cf	carrier fluid or liquid only
gn	Gnielinski's correlation
h	hydraulic
HT	heat transfer
hw	hot water side
hy	hydrodynamic
in	inlet
L	local
m	mean or average
s	solid
sl	solid–liquid or ice slurry
t	thickness
v	volume fraction
w	wall
x	axial position

melting heat transfer investigations include the works of Horibe et al. [4], Ben-Lakhdar et al. [5] and Norgard et al. [6]. As also discussed in [3,7], the previously obtained heat transfer results have not always been consistent, due to possible differences in the experimental conditions such as the type of additives used, ice crystal size, ice fraction, Reynolds number range, channel shape, size and orientation, and wall heat flux conditions.

A number of past studies have attempted to correlate the convective heat transfer data in terms of appropriate non-dimensional variables. Although some of the correlations proposed were preliminary in nature, most of them showed a $Nu = f(Re, Pr, X_s)$ type dependence; however, this functional form was not consistent among all the studies. Also, some of these correlations are highly complicated and not easy to apply, which makes them impractical.

Although several heat transfer models have been proposed, there is still no widely accepted correlation that can satisfactorily describe the melting heat transfer characteristics of ice slurries in circular or non-circular channels. This is perhaps due to the particular experimental systems used and narrow ranges of experimental conditions covered in each investigation. Many of the previous studies did not describe the experimental procedures and findings in sufficient detail, so the observed trends in the heat transfer results could not be clearly explained.

An important aspect of ice slurry flow and heat transfer is the question of non-Newtonian behavior due to the ice crystal agglomeration and possible formation of structures [8–10]. Although some researchers have attempted to correlate the non-Newtonian effects [5,11], their models are either expressed in a non-conventional form, cover a limited range of experimental conditions or predict a zero single-phase heat transfer coefficient when the ice fraction approaches zero.

Furthermore, some of the previous melting ice slurry heat transfer investigations have also employed the Log-Mean-Temperature Difference (LMTD) method to determine the ice slurry heat transfer coefficient [4,6,11]. Nonetheless, as Choi et al. [12] have pointed out, it may be difficult to apply the LMTD method to phase change slurries as the ice fraction and local heat

transfer coefficient may change significantly along the flow direction in the heat exchanger. The second assumption can be quite serious in compact heat exchangers because of the strong entrance effects. Thus, to correctly evaluate the convective heat transfer characteristics of ice slurries in compact heat exchangers, the local heat transfer coefficients should be determined. To this end, the present work attempts to obtain local heat transfer coefficients in the thermally and hydrodynamically developing flow region of a rectangular flow channel during forced convective melting of ice slurries.

For a constant wall heat flux, q''_w, the ice slurry heat transfer coefficient, $h_{sl,x}$, is defined as,

$$q''_w = h_{sl,x}(T_w - T_{sl})_{x,m} \quad (1)$$

where T_w is the local wall temperature and T_{sl} is the local ice slurry bulk temperature, defined as [13],

$$T_{sl,x} = \frac{\int_{A_c} \rho \cdot C_p \cdot u \cdot T \cdot dA_c}{\int_{A_c} \rho \cdot u \cdot C_p \cdot dA_c} \quad (2)$$

where u, C_p, ρ and T are the velocity, heat capacity, density and temperature profiles, respectively, of the ice slurry at a given axial position in the channel. It is evident that the accurate evaluation of the local heat transfer coefficient and ice slurry bulk temperature require knowledge of the ice slurry density (ice fraction), mixture velocity and temperature distributions across the flow channel. Since little information is yet available in the literature regarding ice fraction, velocity and temperature profiles for convective melting of ice slurries, it is thus necessary to conduct these measurements under convective melting conditions.

The main objectives of this study were to obtain reliable heat transfer data and propose heat transfer correlations for vertical upward ice slurry flow in a heated rectangular channel. Ice slurry velocity, ice fraction and temperature profiles were also measured to gain further insights into the ice slurry flow and heat transfer characteristics. The experiments covered laminar ($Re_{cf} < 2100$) and slightly turbulent flow velocities that are typically encountered in each flow channel of compact heat exchangers, unlike some of the previous studies which covered extremely high Reynolds numbers [14,15].

2. Experimental apparatus and procedure

2.1. Experimental facility and test section

The experimental facility consisted of an ice slurry generator (Sunwell, Model: Deepchill^{TM} IG-6VM), continuously stirred ice slurry storage tank, variable speed pump, magnetic flow meter, flow control valve and a data acquisition system. Ice slurry was made by circulating the brine (6.2% NaCl in water) through the ice slurry generator. The mean size of the ice crystals in the ice slurry produced was measured to range from 100 to 200 μm [10]. The details of the experimental apparatus and instrumentation are given in Part I [10], so they will be only briefly described here.

The test section was a rectangular channel, 0.305 m wide and with a gap of 0.025 m (H), formed between a heated brass plate, 0.533 m (L) × 0.305 m (W), and an acrylic wall. The brass plate was heated on its backside by passing warm water through a serpentine coil of 12.7-mm O.D. copper tube with 14 passes. This coil was partially imbedded in grooves machined at 2.54-cm intervals on the back surface of the brass plate. To achieve turbulent ice slurry velocities of up to 0.90 m/s, acrylic plates of appropriate thickness were inserted into the channel to partially cover the brass plate and reduce the flow and heat transfer areas. The hydraulic diameter, D_h, was thus reduced from 0.047 m to 0.023 m. Table 1 summarizes the test section parameters for the two channel configurations used, which are referred to as narrow (partially blocked channel) and wide flow channels, respectively.

2.2. Measurement methods

The average wall heat flux, q''_w, was evaluated from a heat balance performed on the warm water side of the test section taking into account the heat losses to the surroundings,

$$q''_w = \frac{\rho_{hw} \cdot Q_{hw} \cdot C_{p,hw} \cdot (T_{hw,in} - T_{hw,out}) - H_{losses}}{A_{HT}} \quad (3)$$

where Q_{hw} is the volumetric flow rate of the warm water measured using both a rotameter and a turbine flow meter (JLC, Model: IR-Opflow Type 5), and ρ_{hw} and $C_{p,hw}$ are the density and heat capacity, respectively, of the warm water evaluated using the average of the inlet and outlet water temperatures, $T_{hw,in}$ and $T_{hw,out}$, are recorded using T-type thermocouples, and A_{HT} is the brass-to-ice slurry heat transfer area. The heat losses, H_{losses}, were estimated by performing a heat balance on the warm water side and collecting the heat transfer data with an empty test section. The heat losses to the surrounding were determined to be small (*maximum*

Table 1
Plate heat exchanger's geometric configurations

Parameter	Narrow channel	Wide channel
Hydraulic diameter, D_h	0.023 m	0.047 m
Flow area, A_c	0.0013 m^2	0.008 m^2
Heat transfer area, A_{HT}	0.053 m^2	0.163 m^2
Heated length, L	0.533 m	0.533 m
Heated width, W	0.100 m	0.305 m
Channel height (gap), H	0.013 m	0.025 m
Channel aspect ratio, $\alpha^* = H/W$	1:8	1:12

1% to 4% of the total heat removed) but included in the calculation of the ice slurry heat transfer coefficient. The total heat gains at an ambient temperature of 20 °C from the non-insulated front and side acrylic walls were estimated to be approximately 35 W at *maximum*, based on the ice slurry and brine temperatures of −3.5 °C.

The local ice slurry heat transfer coefficient, $h_{sl,x}$ was measured at steady state using several thermocouples installed at different axial and lateral locations in the test section (see Fig. 1). The local bulk temperature of ice slurry, $T_{sl,x}$, was recorded using six 1.56-mm O.D. T-type thermocouples placed midway through the 25.4-mm gap channel. The brass wall temperatures, T_w, were measured using another six 1.02-mm O.D. T-type thermocouples inserted 18.05-mm deep into the 19.05-mm thick brass plate and placed exactly opposite to the ice slurry temperature probes.

In this investigation, the local ice slurry Nusselt number, $Nu_{cf,x}$, was evaluated based on the local heat transfer coefficient ($h_{sl,x}$), the thermal conductivity of the carrier fluid (k_{cf}), and the hydraulic diameter, D_h.

$$Nu_{cf,x} = \frac{h_{sl,x} \cdot D_h}{k_{cf}} \tag{4}$$

Although others have used the mixture thermal conductivity based on Maxwell's equation [16–18], the thermal conductivity of the carrier fluid was employed in the present analysis due to its computational simplicity. Both approaches have certain merits in correlating the heat transfer data as pointed out in [7].

The average ice slurry heat transfer coefficient, $h_{sl,m}$, was computed using the arithmetic average of the local ice slurry heat transfer coefficients. The average ice slurry Nusselt number based on $h_{sl,m}$ was again defined based on the thermal conductivity of the carrier fluid.

Local ice slurry temperature, ice fraction and mixture velocity profiles were measured near the heated brass wall to characterize the behavior of ice slurries flowing in the vertical rectangular channel. The ice slurry temperature profile was obtained by traversing a single 1.56-mm O.D. T-type thermocouple at the plane of symmetry ($z/W = 0.50$) and the axial location of $x \sim 0.373$ m from the inlet of the heated section (see Fig. 1). These temperature distribution measurements were made for both the wide and narrow channel configurations, respectively. Local measurements of the mixture velocity and ice fraction were also conducted using a hot film anemometer (TSI, Model: 1231AR) and an ice slurry sampling probe, respectively, only for the wide channel. The hot film anemometer (HFA) and ice slurry sampling probes were traversed across the channel gap of 25.4-mm at an axial position of $x \sim 0.28$ m from the inlet of the heated section. These measurement methods are extensively described in Part I.

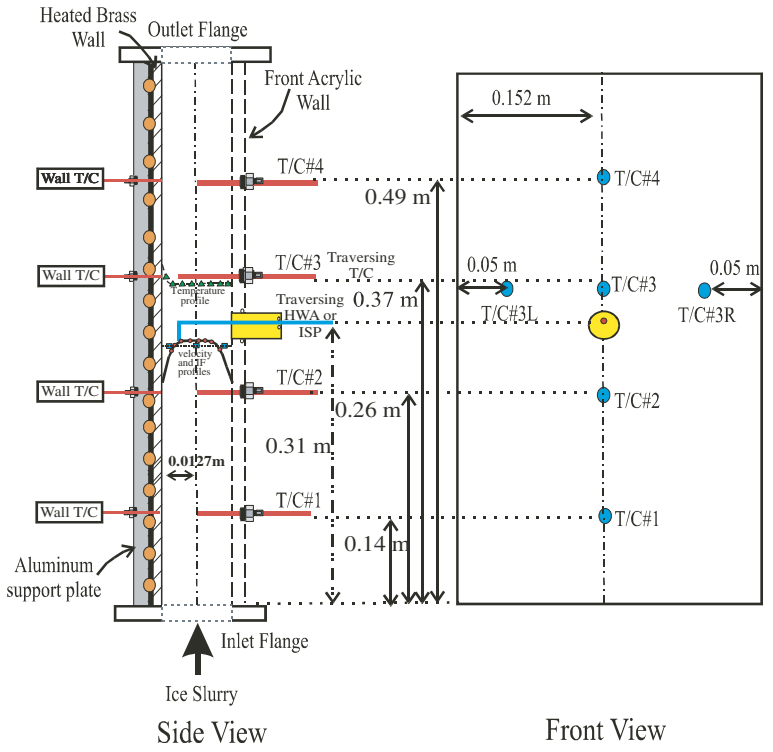

Fig. 1. Thermocouple, HFA and ice slurry (ISP) probe locations in the heated section.

2.3. Test procedure

Experiments were performed by first producing an ice slurry in a storage tank containing an aqueous hypoeutectic solution of 6.2% by weight NaCl in water solution (brine) using a 12-kW refrigerating capacity scraped-surface ice slurry generator. During the melting heat transfer tests, the ice slurry generator was left turned on and its temperature controller was periodically adjusted to vary the ice slurry generation rate so as to maintain a desired ice fraction at the inlet of the test section. The ice slurry was circulated using a variable speed centrifugal pump from the storage tank through the test section, which was heated at a controlled rate by passing warm water on the secondary side thus melting the ice slurry flowing vertically upwards.

In each diabatic run, about 2–3 kg of ice slurry samples were withdrawn from both the inlet and outlet of the test section to obtain the average ice fraction, either Φ_v (volumetric) or X_s (mass) in the test section. The ice fraction of each sample was determined using a batch calorimetry method.

Heat transfer coefficient data were obtained for an extensive range of Reynolds numbers ($Re_{cf} \sim 1800$–11,000) and ice fractions ($X_s = 0$–25%) in both the wide and narrow flow channel configurations. The test matrix consisted of nine ice slurry velocities, six different inlet ice fractions and two wall heat fluxes for a total of 108 experimental runs. For the secondary side, two warm water temperatures of approximately 43 °C and 15 °C were chosen, and the average wall temperature was varied between 1 and 15 °C to impose different average wall heat fluxes. In these experiments, the mass flow rate of warm water on the secondary side was maintained constant at 0.15 kg/s for all diabatic runs.

All the data from the various instruments were recorded using a National Instruments PC (NI-DAQ) based data acquisition board (National Instruments, Model: PCI-MIO-16-E4) consisting of 16 analog input channels, multiplexed with two signal-conditioning modules (National Instruments, Model: SCXI-1102B and SCXI-1125). The steady state heat transfer coefficient data, local ice fraction and temperature distribution data were collected at a sampling rate of 1 Hz, while the HFA velocity data were recorded at 5 Hz.

The heat transfer coefficient and local distribution measurements were made during steady state, which was indicated by the minimal changes observed in the ice slurry flow rate, average ice fraction, and ice slurry temperatures, recorded by the data acquisition system.

2.4. Uncertainty estimates

Uncertainty estimates for the measurements are based on a propagation of error analysis. The experimental uncertainties of time-averaged magnitudes of local ice fraction and local streamwise velocity are ±10% and ±2.5% (0.60 cm/s), respectively. The latter uncertainties were established from bench scale calibration tests as described in Part I [10]. An end-to-end calibration was performed on the test section thermocouples through the NI-DAQ under adiabatic single-phase liquid and ice slurry flow conditions. This yielded a maximum absolute uncertainty in the temperature measurements of ±0.15 °C. The error in the location of the traversible sensors (ice slurry probe, thermocouple and HFA) was determined from in situ calibrations to be about 0.50 mm (or 2%).

The variations of the wall temperatures and wall heat fluxes around the averaged values were determined to be 0.02–0.15 °C and 400–700 W/m^2, respectively. These errors were established by examining the data from experimental runs with the maximum and minimum flow rates, ice fractions and imposed wall heat flux conditions. The greatest experimental uncertainties occurred for the experimental runs conducted at low wall heat fluxes and high ice fractions ($X_s = 25$ wt%) as certain local wall temperatures reached around 0 °C; however, this uncertainty did not greatly influence the accuracy in the evaluation of the local heat transfer coefficient as the temperature difference, $T_w - T_{sl}$, defined in Eq. (1) was always sufficiently high (between 4 and 5 °C at minimum). The estimated maximum uncertainty in the time-averaged local heat transfer coefficient, $h_{sl,x}$, was between 8% and 11%. The corresponding absolute error in the value of local Nusselt number, $Nu_{cf,x}$, was about 5–10. The uncertainty in the Reynolds number was approximately ±2.5%.

3. Results and discussion

3.1. Local distributions near a heated wall

3.1.1. Ice slurry velocity

Fig. 2(a) compares the non-dimensionalized ice slurry velocity distributions near a heated and unheated wall for runs conducted with similar ice fractions ($\Phi_v \sim 5$–6 vol.%) and Reynolds numbers ($Re_{cf} \sim 4000$) but different wall heat fluxes, q''_w. In this figure and hereafter, each local velocity data point represents the time-averaged velocity of about 100 HFA readings made at a sampling rate of 5 Hz over a period of 20 s during the melting or adiabatic experiments. Also given in this figure is the average wall heat flux, local Nusselt number for the melting runs and the Reynolds numbers based on the carrier fluid (liquid) properties, Re_{cf}, and homogeneous ice slurry mixture properties, Re_{sl}, as defined in Part I [10].

For the results given in Fig. 2(a), the average ice slurry velocity, V, obtained by integrating the velocity profile data, matched the mean ice slurry velocity, $\langle u_{sl} \rangle$,

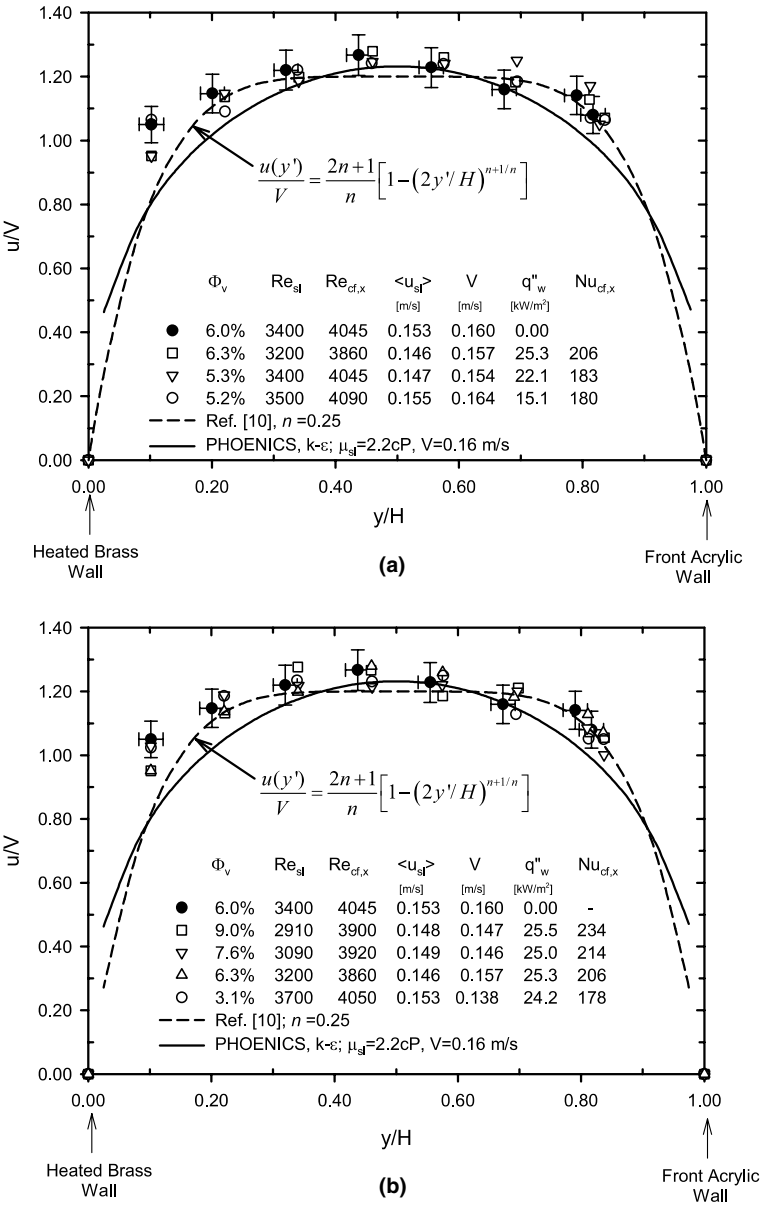

Fig. 2. Dimensionless ice slurry velocity profiles: (a) effect of q''_w and (b) effect of ice fraction for $Re_{cf} \sim 3900$ and $q''_w \sim 25\ kW/m^2$.

to within 5%. Fig. 2(a) also compares the measured velocity profile data with the adiabatic laminar velocity profile for a power law non-Newtonian fluid with $n = 0.2$ as given in Part I [10], and the velocity profile predicted using a PHOENICS code with Thomas's viscosity correlation [19] for a flow between two parallel plates.

The general qualitative features of these velocity profiles suggest that when a wall heat flux is imposed, the flow near the heated wall decelerates in comparison to an adiabatic ice slurry flow, while in the core region the velocity is unaffected by heating. The velocity reduction near the heated wall is probably due to the disappearance of ice crystals in the region close to the heated wall. This region is referred to as the "ice free" layer that has on average a greater density than the bulk ice slurry. When a higher wall heat flux is imposed, the velocity near the heated wall is further reduced by about 10% as Fig. 2(a) illustrates. Although we have not confirmed the existence of the "ice free" layer in the present experiments and do not know how thick it is, it is plausible that such a layer would occur under sufficiently high heat flux conditions in the thermally developed region. It is distinguished from the thermal boundary

layer in which the temperature may be higher than the melting point although the ice fraction is not zero. Such a thermal non-equilibrium phenomenon between the ice crystals and carrier fluid has been observed in ice slurry flows previously [6,11].

At the low ice slurry velocities tested ($\langle u_{sl} \rangle$ = 0.1–0.15 m/s), the free-convection effects become important according to Metais and Eckert [20], so that although ice slurry viscosity is reduced as ice fraction decreases near the heated wall, the reduced velocity data indicate that the density effect is more dominant than that of viscosity. Since the density of water increases with temperature above the melting point up to 4 °C, any temperature increase in the "ice free" layer would increase the fluid density and decelerate the ice slurry flow close to the heated wall. Most velocity distribution data near the heated wall showed a systematic 10% reduction in comparison to adiabatic ice slurry flow, which is larger than the 5% uncertainty in the velocity measurement. Thus, the present velocity profile measurements suggest that forced convective heating and melting of the ice slurry can decelerate the flow near the heated wall at low velocities.

Fig. 2(b) shows the effect of the average ice fraction on the ice slurry velocity profile near the heated wall for $Re_{cf} \sim 3900$ and $q''_w \sim 25\ kW/m^2$. This figure shows no clear effect of the average ice fraction on the velocity near the heated wall. Although the ice fraction range investigated was small, the local heat transfer coefficient represented by $Nu_{cf,x}$ improved as the ice fraction increased.

3.1.2. Temperature profiles

Fig. 3(a) shows typical ice slurry temperature profiles across the heated channel for $Re_{cf} \sim 3800$ and volumetric ice fractions up to 26% obtained in a wide channel (α^* = 1:12). These temperature profiles are plotted as a function of the dimensionless distance, y/H, measured from the surface of the heated brass wall ($y/H = 0$). Each temperature data point shown in this figure and hereafter represents the time-average of 20 data points obtained over a period of ~10 s at a specified ice fraction. Also for these temperature profiles and hereafter, the temperature rise near the acrylic wall ($y/H \geqslant 0.7$) is considered to be anomalous due to the effect of heat conduction along the thermocouple sheath. Upon careful examination, the temperature data for $y/H < 0.6$ can be considered to be unaffected by conduction effects and satisfactorily represent the ice slurry temperature increase near the heated wall.

The temperature profiles obtained in a wide channel (α^* = 1:12) reveal that the thermal boundary layer is thin even at low ice fractions and the ice slurry temperature remains fairly uniform across most of the flow channel regardless of the ice fraction ($X_s \sim 2$–24%). In view of the blunt velocity profiles obtained and discussed earlier, the *bulk ice slurry temperature*, T_{sl}, can be assumed to be given by the temperature in the middle of the flow channel, which eliminates the need to evaluate the integrals given in Eq. (2).

Fig. 3(b) shows typical temperature profiles obtained in a narrow channel under turbulent flow conditions ($\langle u_{sl} \rangle$ = 0.90 m/s, $Re_{cf} \sim 11{,}000$), at mean ice fractions up to 24 vol.%. These results suggest that at high ice slurry velocities, the "ice free" layer near the heated wall is estimated to be less than 1 mm in thickness, much thinner than those observed at lower velocities. This suggests that the mechanism of turbulent heat transfer in ice slurry flows may be strongly influenced by both the turbulent eddies and ice crystals which disturb the thermal boundary layer and increase the heat transfer coefficient with increasing ice fraction and Reynolds number. This will again be discussed later.

3.1.3. Ice fraction profiles

In Part I [10], the ice fraction distributions were presented for the case of adiabatic ice slurry flow in a vertical rectangular channel. In this work, the ice fraction variation near a heated wall is examined as the ice fraction profiles have previously been hypothesized to influence the local heat transfer characteristics in horizontal channels [4,21,22]. However, to our knowledge, ice fraction profile measurements near a heated wall have never been reported before, thus the present work provides a new set of data needed for the design of ice slurry heat exchangers.

Fig. 4 shows the effect of the mean ice fraction on the normalized local ice fraction profile data (Φ/Φ_m) near a heated wall at $Re_{cf} \sim 3800$ and $q''_w \sim 24\ kW/m^2$. These normalized plots are similar to those presented in Part I [10] for the adiabatic flow case; however, the local ice fraction in the vicinity of the heated wall is approximately 5–20% lower than in the bulk, while it is higher near the opposite adiabatic wall ($y/H \sim 0.75$) than in the bulk for dilute ice slurry runs ($3\% < \Phi_v < 8\%$) as in the adiabatic flow results. Beyond the measurement uncertainty in the ice fraction measurement, a local ice fraction peaking phenomenon near the adiabatic wall was systematically observed, but disappeared at the heated wall ($y/H = 0$) for all dilute ice slurry runs conducted. At higher mean ice fractions (i.e., $\Phi_v >$ 10 vol.%), however, the peaking phenomenon disappeared even near the adiabatic wall. The peaking of the local ice fraction near the adiabatic wall is consistent with visual observations of ice crystals migrating from the free stream towards the adiabatic wall. Nonetheless, a more detailed local ice fraction measurement is needed to verify the current values of the local ice fraction peaks near the adiabatic wall.

In Fig. 4, the local ice fraction near the heated wall does not show any systematic variation with increasing ice fraction in the bulk. Similar results were also

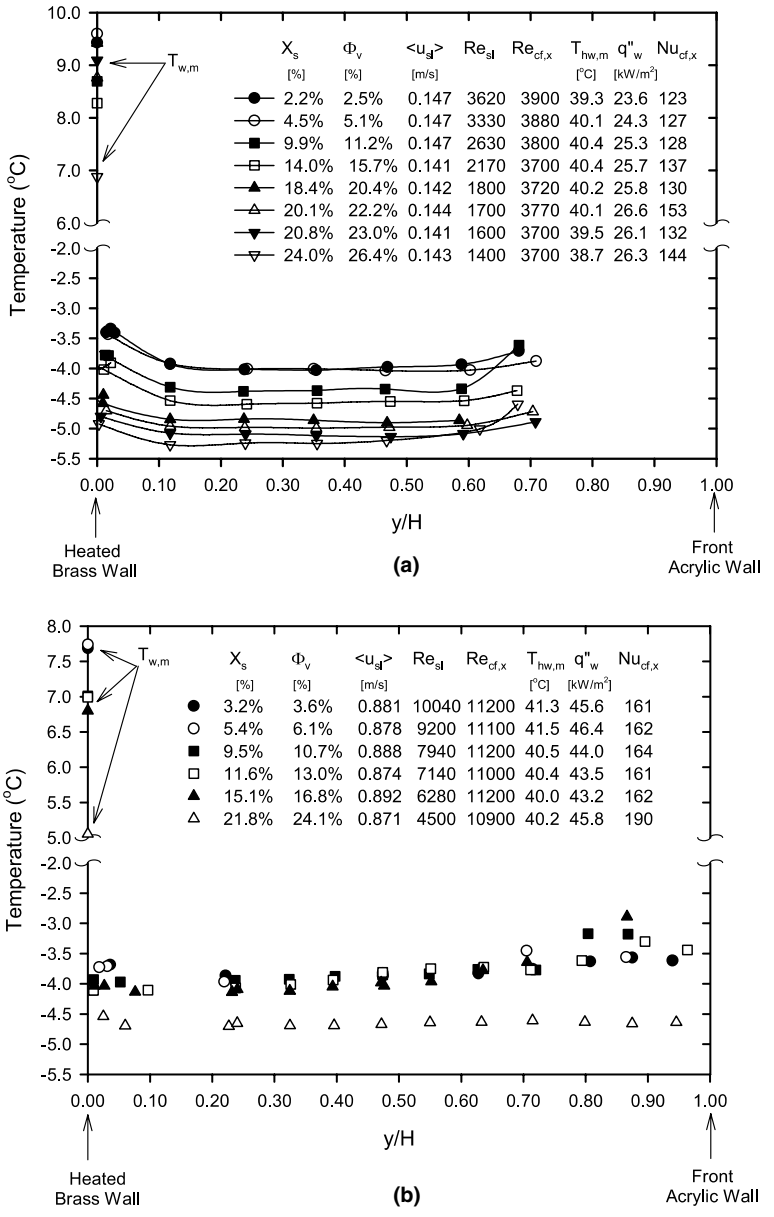

Fig. 3. Ice slurry temperature distributions for: (a) $Re_{cf} = 3800$ and $\alpha^* = 1{:}12$ and (b) for $Re_{cf} \sim 11{,}000$ and $\alpha^* = 1{:}8$.

obtained at another Reynolds number of 2700 [23]. These results may suggest that even at low ice fractions and velocities, the "ice free" layer remains thin as the ice crystals in vertical flows tend to disperse in a uniform fashion across the heated channel. In comparison to adiabatic ice fraction profiles, however, the ice fraction was reduced near the heated wall in dilute ice slurries ($\Phi_v < 8$ vol.%) and the reduction was approximately 10–20% of the bulk ice fraction. On the other hand, in the more concentrated ice slurries ($\Phi_v > 10$ vol.%), the ice crystals were more closely packed so that the ice fraction reduction near the heated wall was by only 5–10% of the bulk ice fraction. This reduction in the ice fraction near the heated wall would, in turn, impact the local heat transfer coefficient as will be discussed next.

3.2. Heat transfer characteristics

3.2.1. Local heat transfer characteristics

In Fig. 5, the streamwise evolution of the local Nusselt number, $Nu_{cf,x}$, is plotted against x/D_h for $Re_{cf} = 6.6 \times 10^3$, average ice fractions of $X_s \sim 5.8\%$, 10% and 20%, and two different wall heat fluxes, q''_w. The

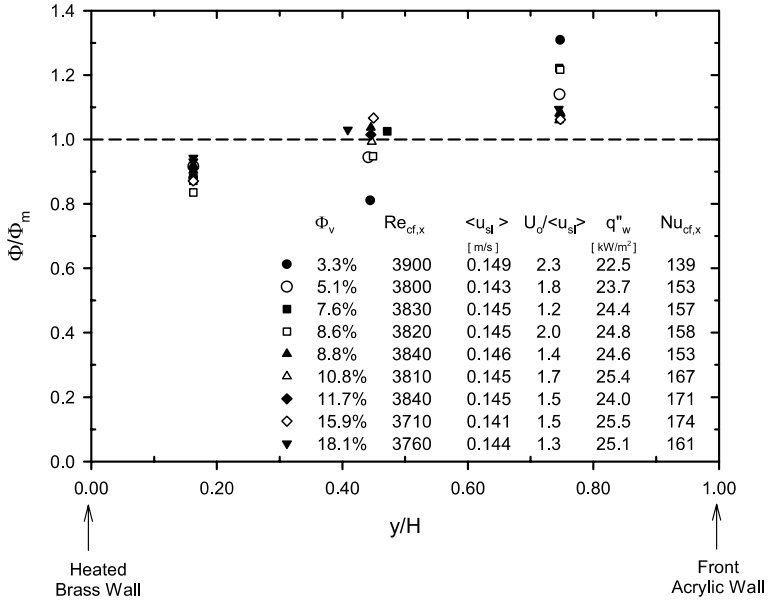

Fig. 4. Effect of Φ_v on ice fraction distribution at $Re_{cf} \sim 3800$ near a heated wall.

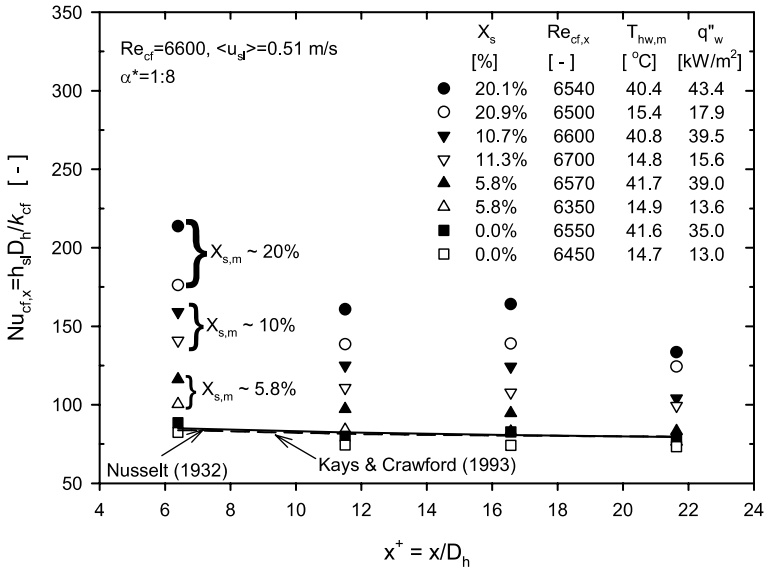

Fig. 5. Effect of wall heat flux on local Nusselt number for $Re_{cf} \sim 6600$, $\langle u_{sl} \rangle \sim 0.51$ m/s and $\alpha^* = 1{:}8$.

corresponding single-phase Nusselt numbers (X_s = 0.0%) with nearly similar wall heat fluxes and Reynolds numbers as the ice slurry runs are also plotted in Fig. 5. The local Nusselt numbers given in these figures and hereafter represent the steady state values, time-averaged over a period of approximately 2–4 min for a specified ice fraction.

In Fig. 5, an excellent agreement is found between the measured single-phase Nusselt numbers (at $T_b \sim -3$ °C) and the analytical solution provided by Kays and Crawford [24] for a thermally developing turbulent flow between parallel plates (reported for $Re = 7096$, $Pr = 10$) where one plate is maintained at a uniform heat flux while the other plate is insulated. As also indicated in this figure, an excellent agreement was also found between the measured single-phase heat transfer values and those predicted by Nusselt's correlation [25], which is extensively used to predict the heat transfer coefficients in the entrance region of turbulent flows [26,27]:

$$Nu = 0.036 Re_{cf}^{0.80} \cdot Pr_{cf}^{1/3} \left(\frac{D_h}{x}\right)^{0.055} \quad 10 < \frac{x}{D_h} < 400 \qquad (5)$$

Fig. 5 clearly illustrates that at any given axial location, x/D_h, the local Nusselt number progressively increases with increasing ice fraction and wall heat flux. Furthermore, the Nusselt numbers are higher at the inlet of the heat transfer section ($x/D_h = 6.4$) since the flow is still developing there, and $Nu_{cf,x}$ slowly decreases towards the exit of the heat exchanger ($x/D_h \sim 22$) as the flow becomes more thermally developed.

In Fig. 5, the local convective heat transfer coefficients in the thermally developing region are seen to increase by up to 300% as the mass ice fraction is increased to 20%. This increase is attributed to the ice crystals flowing near the heated wall which limit the growth of the thermal boundary layer. At high ice fractions, the ice crystals are more closely packed and tend to diffuse towards the heated wall, reducing the thermal boundary layer thickness as compared to the case of low ice fractions as illustrated schematically in Fig. 6.

The effect of wall heat flux on the heat transfer coefficient can also be observed in Fig. 5. In fully developed single-phase turbulent flows where small to moderate temperature differences existed between the heated wall and the fluid, the local Nusselt number was only weakly dependent on the wall heat flux as seen in the zero ice fraction data shown in Fig. 5 [28]. However, for ice slurry flows at different wall heat fluxes but similar ice fractions, the local Nusselt number increased by about 10–30% when a higher wall heat flux was imposed. This wall heat flux effect may be attributed to the occurrence of slightly larger temperature gradients near the heated wall induced again by the ice crystals flowing near the heated wall as further explained below.

As the wall heat flux is increased, more ice crystals will melt and the local ice fraction will be reduced near the heated wall. This should cause the thermal boundary layer to grow in thickness. However, when the bulk ice concentration is sufficiently high (e.g., $\Phi_v > 10\%$), ice crystals will tend to spread across the channel and migrate towards the heated wall, thereby countering the effect of increased melting near the wall. Thus, when the wall heat flux is increased, the thermal boundary layer will not become as thick as it would if there were no ice crystals present. This limited increase in the thermal boundary layer thickness would result in a steeper temperature gradient and larger convective heat transfer coefficient at higher wall heat fluxes as seen in Fig. 5. As the flow becomes more thermally developed further downstream, the thermal boundary layer becomes thicker and the influence of the ice crystals on the thermal boundary layer gets diminished, so the heat transfer coefficient is less affected by the increasing wall heat flux, as seen in the present data obtained at $x/D_h \sim 22$.

At extremely high wall heat fluxes, melting of the ice crystals and the reduction in the local ice fraction near the heated wall would be more significant, so the thermal boundary layer thickness would increase resulting in a reduced heat transfer coefficient. This hypothesis is consistent with the degradation of ice slurry heat transfer coefficient at extremely high wall heat fluxes ($q''_w > 100\ \mathrm{kW/m^2}$) observed previously by Snoek and Bellamy [14].

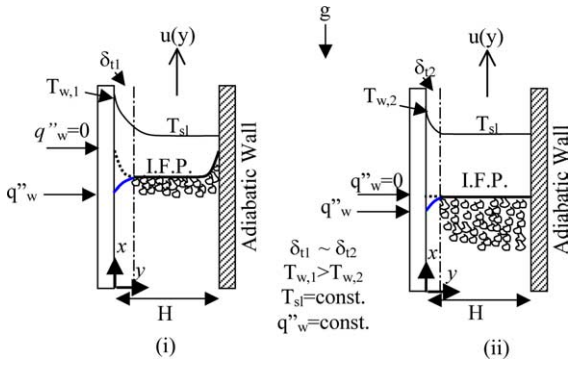

Fig. 6. Possible explanation of the effect of ice fraction profile (I.F.P.) on the local heat transfer coefficient at (i) low ice fractions ($3\% < \Phi_v < 8\%$), and (ii) high ice fractions ($\Phi_v > 10\%$).

3.2.2. Average heat transfer coefficients

The average ice slurry Nusselt numbers are plotted in Fig. 7 for runs conducted at different Reynolds numbers and wall heat flux conditions but a similar ice fraction $X_s \sim 20\%$, in both the narrow and wide channel configurations. Fig. 7 illustrates no significant influence of the wall heat flux on the average single-phase heat transfer coefficients. The experimental single-phase heat transfer coefficients are also well predicted by the correlation given by Gnielinski [29,30] in the transition Reynolds number range between 2300 and 10^4,

$$Nu_{gn,m} = \frac{(f/2) \cdot (Re_{cf} - 1000) \cdot Pr_{cf}}{1 + 12.7 \cdot \sqrt{(f/2)} \cdot (Pr_{cf}^{2/3} - 1)} \qquad (6)$$

As also previously reported in the local heat transfer coefficient results, the average ice slurry Nusselt numbers are greater than those in single-phase convection. The average ice slurry Nu numbers are further augmented by about 15–20% when the applied heat flux is approximately doubled. Generally, the degree of heat transfer enhancement due to the wall heat flux applied is constant over the Reynolds number range investigated as is illustrated in Fig. 7.

From all the previous ice slurry melting heat transfer investigations discussed in [2,3], only Kawanami et al. [21] noticed a similar heat transfer enhancement (15–25%) in their local heat transfer values when the heat

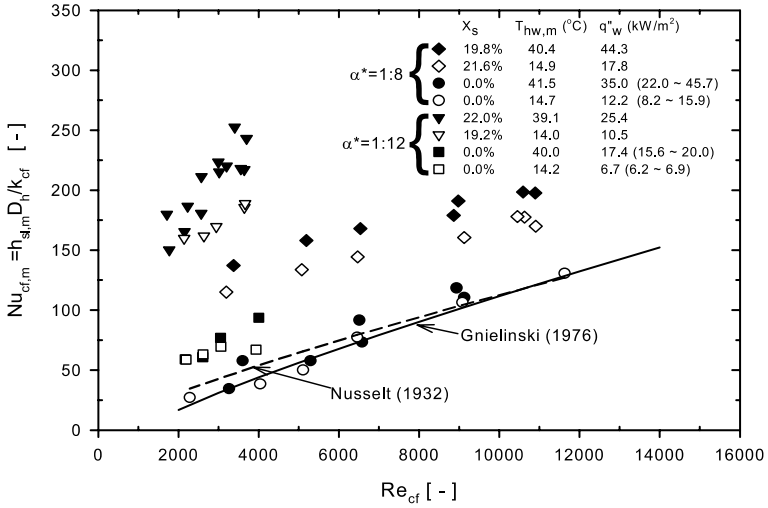

Fig. 7. Effect of wall heat flux on Nusselt number at $X_s \sim 20\%$.

flux was also doubled ($q''_w = 4$–8 kW/m^2) in a top heated horizontal rectangular duct, while Jensen et al. [11] only stated in their study using a horizontal cylindrical heat exchanger that the imposed wall heat flux did not affect the overall heat transfer coefficient. On the other hand, Snoek and Bellamy [14] reported degradation of the ice slurry heat transfer coefficient in comparison to single-phase convection at high Reynolds numbers ($Re_{cf} >$ 80,000) and high wall heat fluxes ($q''_w > 100$ kW/m^2) for a 19-mm I.D. tubular heat exchanger. To our knowledge, no other melting heat transfer studies have reported the effect of wall heat flux on the average heat transfer coefficient for ice slurries.

In this study, the 3–4 times higher average heat transfer coefficients obtained in the wide channel ($\alpha^* = 1{:}12$) in comparison to single-phase convection are attributed to a combination of the free-convection effects and shorter thermal entrance lengths. These free-convection and thermal entry effects are inherent in short compact heat exchangers, and lead to improved heat transfer coefficients.

Fig. 7 also suggests that the average ice slurry heat transfer coefficient data for a narrow channel clearly comply with the turbulent convection correlation, while the results for the wide channel do not, even for runs with identical Reynolds numbers and ice fractions as the narrow channel. For the wide channel, the presence of non-Newtonian flow characteristics, mixed-convection effects and shorter thermal entry lengths result in exceptionally augmented ice slurry heat transfer coefficient values. Thus, for the heat transfer results obtained in the wide channel, $\alpha^* = 1{:}12$, correlating the ice slurry heat transfer data is not straight forward and requires additional efforts. Due to this complexity, empirical heat transfer correlations have been developed as described below.

3.2.3. Heat transfer correlations

3.2.3.1. Turbulent heat transfer correlations. A dimensionless correlation is required for design purposes to predict convective melting of ice slurry flows in heated channels. In this work, the following dimensionless variables are used to correlate the convective heat transfer data accounting for the effect of ice crystals: the average Nusselt number ($Nu_{cf,m}$), Reynolds number (Re_{cf}), Prandtl number (Pr_{cf}), average ice fraction (X_s) and viscosity ratio between the bulk carrier fluid and the wall, μ_{cf}/μ_w. The wall and bulk viscosities are evaluated at the corresponding wall and ice slurry bulk temperatures, respectively. A multiple, linear regression analysis was performed on the average heat transfer coefficient data. In this correlation, the heat transfer data only from the narrow channel were used as they were free of natural convection effects. The coefficients of the proposed regression model were determined using the method of least squares, which yielded the following correlation giving the best fit to the present experimental data for $3300 < Re_{cf} < 11{,}000$ and $0.0 < X_s < 0.25$:

$$Nu_{sl,m} = \frac{h_{sl,m} \cdot D_h}{k_{cf}} = Nu_{gn,m}[1 + 1.85 \times 10^5 \cdot X_s^{0.72} \cdot Re_{cf}^{-1.30}(\mu_{cf}/\mu_w)^{2.47}] \quad (7)$$

In Eq. (7), Nu_{gn} is the single-phase Nusselt number predicted by Gnielinski's [29,30] variable property heat transfer correlation for the entrance region given by Eq. (6).

Fig. 8(a) compares the experimental heat transfer results with those predicted by Eq. (7). Unlike some of the other ice slurry heat transfer correlations given in Ref. [2], this proposed heat transfer correlation is also applicable when the ice fraction approaches zero. Furthermore, the proposed heat transfer correlation is simpler

to apply as it only involves four parameters (X_s, Re_{cf}, Pr_{cf}, μ_{cf}/μ_w) and the heat transfer properties are based on the carrier fluid properties.

Fig. 8(a) also shows the predictions by heat transfer correlations proposed by Horibe et al. [4] and Jensen et al. [11], which covered similar ice fraction and Reynolds number ranges as the present study. The differences between the proposed heat transfer correlation and the present heat transfer data are attributed to the shorter thermal entry lengths involved in the current study. The shorter thermal entry lengths involved in compact heat exchangers will yield higher heat transfer coefficients. In addition, the previously proposed heat transfer correlations were based on the Log-Mean-Temperature Difference, so one needs to properly determine the thermal resistance on the warm fluid-side and the heat transfer surface area to extract the ice slurry-side heat transfer coefficient.

As a concluding remark on turbulent ice slurry convection, none of the previous heat transfer studies would be

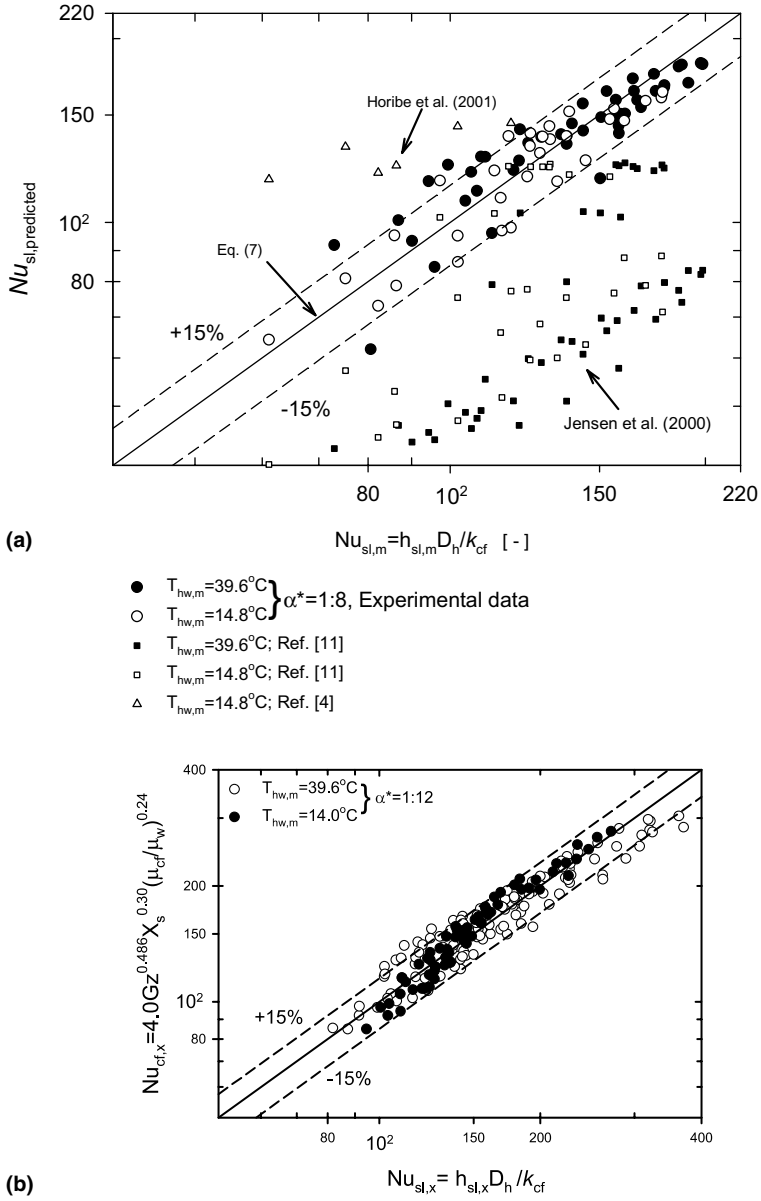

Fig. 8. Comparison of experimental results and proposed empirical correlations for (a) average Nusselt numbers for turbulent convection to ice slurries and (b) local Nusselt numbers for laminar convection to ice slurries.

applicable to the short thermal entry lengths involved in the present compact heat exchanger geometry. In this regard, since multiple channels connected in parallel will be used in compact heat exchangers, the flow would be typically laminar or slightly turbulent, unlike in Snoek and Bellamy's [14] experiments involving extremely high turbulent flows ($Re_{cf} > 35{,}000$). Thus, the present heat transfer correlation, Eq. (8), is currently, in our knowledge, the only turbulent convection correlation useful for the development of compact heat exchangers for ice slurry utilization.

3.2.3.2. Laminar heat transfer correlation. Fig. 8(b) shows a local heat transfer correlation developed for laminar ice slurry flow in a wide channel, $\alpha^* = 1{:}12$. For the low ice slurry velocities involved ($\langle u_{sl} \rangle < 0.15$ m/s), the mixed-convection effect and non-Newtonian flow characteristics would become more prevalent as previously discussed. For the laminar convection correlation, the dimensionless variables used are the local Nusselt number ($Nu_{cf,x}$), Graetz number ($Gz = Re_{cf} Pr_{cf} D_h/x$), the average ice fraction (X_s) and the viscosity ratio between the bulk fluid and the wall, μ_{cf}/μ_w. The coefficients of the proposed regression model were determined using the method of least squares and 180 independent experimental data points, which yielded the following correlation giving the best fit to the present experimental data for $2100 < Re_{cf} < 4000$, $0.01 < X_s < 0.25$ and $GrPr_{cf}(D_h/x) > 10^6$:

$$Nu_{cf,x} = 4.0 Gz^{0.486} X_s^{0.30} (\mu_{cf}/\mu_w)^{0.24} \quad (8)$$

Fig. 8(b) compares the present heat transfer results with those predicted by Eq. (8). All the data can be predicted by Eq. (8) to within ±15%. A similar heat transfer formulation was first reported by Ben-Lakhdar et al. [5] for ice slurry flows in a short tube without the viscosity ratio, μ_{cf}/μ_w. The heat transfer correlation proposed by Ben-Lakhdar et al. [5] could not collapse the current heat transfer data into a single line as a different definition of the Graetz number was used in [5]. The newly proposed correlation given by Eq. (8) eliminates this problem as the Graetz number is defined based on the carrier fluid properties.

The new heat transfer correlation given by Eq. (8) is again to our knowledge the only laminar convection correlation currently available that would be useful for the development of new compact heat exchangers consisting of multiple parallel plates for ice slurry utilization at low flow velocities.

3.2.4. Comparison with other work

The conflicting heat transfer results produced by different researchers reviewed in [2,3] and also encountered in the present investigation, point to the importance of a number of functional parameters that could affect the behavior of ice slurries including the mixture viscosity, Reynolds number, ice crystal size and ice fraction, additive type and concentration, and heat flux. The current investigation has also suggested that the thermally developing flow conditions and corrugated or smooth surfaces could contribute to these discrepancies. Here we also briefly examine and comment on these factors.

Fig. 9 shows the ratio of Nusselt numbers for ice slurry to chilled water convection heat transfer and compares the results obtained for different channel geometries, Reynolds numbers, thermal entry lengths and ice slurry types [3–6,14,15,31–33]. This plot is merely used for illustrative purposes only and is not meant to provide an absolute comparison basis for all the melting ice slurry heat transfer results, as certain factors (e.g., the ice crystal sizes and channel geometry) could not be taken into consideration. An absolute comparison basis may not be feasible as of this moment since some of the previous studies were preliminary in nature or had missing information. For those studies with missing information, only their high and low limits are compared in the figure.

Fig. 9 illustrates that the heat transfer results of the current investigation are consistent with those reported by Ben-Lakhdar et al. [5] and Jensen et al. [11] for smooth horizontal tubes. In addition, some of the heat transfer results obtained by Christensen and Kauffeld [31] fall in the boundaries of the current work. Thus, for the Reynolds number range between 1000 and 11,000, most of the heat transfer studies conducted in horizontal tubes and vertical smooth plate heat exchangers (current study) suggest that the ice crystals in the ice slurry contribute to 1.2–5 times enhancement in heat transfer coefficients compared to chilled water. On the other hand, the heat transfer studies performed by Snoek and Bellamy [14] and Knodel et al. [15] at much higher Reynolds numbers ($Re_{cf} > 35{,}000$–$80{,}000$) in smooth horizontal tubes suggest a reduction in the ice slurry heat transfer coefficient compared to chilled water convection as illustrated in this figure. At moderate heat fluxes, this reduction in the ice slurry heat transfer coefficient was explained by [15] to be due to the transition from turbulent to laminar flow when the ice fraction is increased, while at high heat fluxes ($q''_w \sim 114$ kW/m^2) the heat transfer degradation was attributed to an increase in the thermal boundary layer thickness [14].

Although the present results were conducted at $Re_{cf} < 11{,}000$, they show a *decreasing trend* in the ice slurry heat transfer coefficient values relative to chilled water at higher Reynolds numbers that may approach values similar to those reported by Snoek and Bellamy [14] and Knodel et al. [15]. Thus, Fig. 9 reinforces the fact that in the practical use of ice slurries in heat exchanger systems, laminar or slightly turbulent flow velocities are preferred in order to provide augmented heat transfer coefficients and reduced pumping requirements compared to chilled water systems.

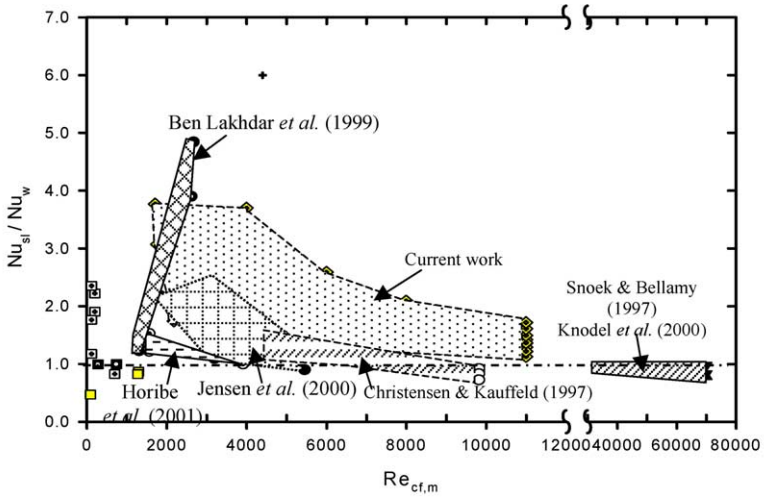

- Jensen *et al.* (2000) [11]; tubular 21/16/12 mm I.D.; 10% ethanol/water; q"$_w$= 8-40 kW/m^2; L/D$_h$= 50-83.
- Ben Lakhdar *et al.* (1999) [5]; tubular 30 mm I.D.; 11% ethanol/water; q"$_w$=12 kW/m^2; L/D$_h$ ~ 15.
- Horibe *et al.* (2001) [4]; tubular 14 mm I.D.; C$_a$=0.0%; L/D$_h$=143.
- Christensen and Kauffeld (1997) [31]; tubular 21.6 mm I.D.; 10% ethanol/water; q"$_w$=6-14 kW/m^2; L/D$_h$ ~ 46.
- Sari *et al.* (2000) [33]; tubular 23 mm I.D.; 10% ethanol/water; L/D$_h$ ~ 43.
- Snoek and Bellamy (1997) [14]; tubular 19 mm I.D.; 8-10% ethylene/glycol; q"$_w$=28-114 kW/m^2; L/D$_h$ ~ 105.
- Knodel *et al.* (2000) [15]; tubular 24.0 mm I.D., C$_a$=0.0%; q"$_w$=15-40 kW/m^2; L/D$_h$ ~ 200.
- Gupta and Fraser (1990) [32]; finned-plate HX, D$_h$ ~ 4.2 mm; 6% ethyelene/glycol.
- Norgard *et al.* (2001) [6]; finned-plate HX, D$_h$=4.0 mm; 16% propylene/glycol.
- Bellas *et al.* (2002) [3]; finned-plate HX; D$_h$=4.0 mm; 5% propylene/glycol.
- Current work (2003) [23]; flat plate HX; D$_h$=22.5 & 47.0 mm; 6.2% NaCl/water; q"$_w$=10-40kW/m^2;L/D$_h$=11-22.

Fig. 9. Ratio of ice slurry Nusselt number to chilled water at different Reynolds numbers obtained by various researchers.

Fig. 9 also reveals that the studies of Bellas et al. [3], Norgard et al. [6], and Gupta and Fraser [32] conducted in commercial plate-type corrugated heat exchangers at low Reynolds numbers ($Re_{cf} < 1000$) have produced conflicting results. Since none of these investigations addressed the effect of corrugations on the heat transfer, it can only be hypothesized that the presence of corrugations at these low Reynolds number ranges ($100 < Re_{cf} < 1000$) may have augmented the heat transfer coefficients for chilled water to values higher than those achieved for ice slurry as the presence of ice crystals in the ice slurry would increase the mixture viscosity and thus diminish the turbulence intensity levels. Unless the effects of corrugations on convection heat transfer are fully addressed and clarified, these conflicting results in commercial plate heat exchangers should be regarded as highly system specific and may be of limited value.

4. Conclusions

An experimental study was performed in the laminar and turbulent flow velocity ranges ($2100 < Re_{cf} < 11{,}000$ based on the liquid properties) for an ice slurry flowing vertically upwards in a rectangular channel with one heated wall for two different channel aspect ratios of 1:12 and 1:8. At steady state, the local ice slurry heat transfer coefficients were measured and reported. To gain more insights into the flow properties of ice slurries and their heat transfer characteristics, local measurements of the axial mixture velocity, temperature and ice fraction distributions were successfully performed under diabatic flow conditions using a hot film anemometer (HFA), a traversing thermocouple probe, and a newly devised on-line ice fraction measurement system based on sampling and calorimetry principles, respectively. The effects of ice fraction, Reynolds number and wall heat flux on the local distributions measurements and the local melting heat transfer characteristics were explored. The major conclusion from the convective melting heat transfer experiments concerns the enhancement effects of ice slurries in compact heat exchangers in comparison to single-phase flow. These effects were shown to consist of four main elements: (1) the high effective heat capacities of ice slurries due to the presence of ice crystals, (2) the thermally and/or hydrodynamically developing flows encountered in compact heat exchangers, (3) the mixed-convection and (4) the non-Newtonian flow characteristics experienced at low flow velocities and Reynolds numbers ($Re_{cf} < 4000$).

All these factors were shown to elevate the heat transfer coefficient of ice slurries to values 1.2–4 times above those obtained in purely single-phase convective flows.

A new turbulent heat transfer correlation was proposed from appropriate dimensionless groups used in conventional turbulent convection correlations that could satisfactorily predict the average heat transfer data to within ±15%. A new local heat transfer correlation was also proposed for the laminar convection range using appropriate dimensionless groups that could predict the local heat transfer data to within ±15%. The novelty of these new heat transfer correlations is that they are simple to use, cover a practical range, predict heat transfer coefficients even for flow without ice crystals, and can thus be useful for the development of new compact heat exchangers for the ice slurry utilization.

Acknowledgement

This project has been financially supported by a CRD grant from the Natural Sciences and Engineering Research Council of Canada. The authors also would like to thank Sunwell Engineering Technologies for partially funding this project and the use of their space and facilities. The financial support from the Government of Ontario through the OGS-ST Scholarship for E.S. is also gratefully acknowledged.

References

[1] B.S. Field, M. Kauffeld, K. Madsen, Use of ice slurry in supermarket display cabinet, Int. Congr. Refrig., ICR0004, 16–23 August 2003, Washington, DC.

[2] V. Ayel, O. Lottin, H. Peerhossaini, Rhelogy, flow behaviour and heat transfer characteristics of ice slurries: a review of the state of the art, Int. J. Refrig. 26 (2003) 95–107.

[3] J. Bellas, I. Chaer, S.A. Tassou, Heat transfer and pressure drop of ice slurries in plate heat exchangers, Appl. Therm. Eng. 22 (2002) 721–732.

[4] A. Horibe, H. Inaba, N. Haruki, Melting heat transfer of flowing ice slurry in a pipe, in: S. Fukusako (Ed.), Proceedings of the Fourth Workshop on Ice Slurries of IIF/IIR, Int. Inst. of Refrigeration, 2001, Osaka, Japan, pp. 145–152.

[5] M.A. Ben-Lakhdar, J. Guilpart, A. Lallemand, Experimental study and calculation method of heat transfer coefficient when using ice slurries as secondary refrigerant, Heat Technol. 17 (2) (1999) 49–55.

[6] E. Norgard, T.A. Sorensen, T.M. Hansen, M. Kauffeld, Performance of components of ice slurry systems: pumps, plate heat exchangers, fittings, in: Proceedings of the Third Workshop on Ice Slurries of IIF/IIR, Int. Inst. Refrigeration, 16–18 May 2001, Horw/Lucerne, Switzerland, pp. 129–136.

[7] E. Stamatiou, M. Kawaji, Heat transfer characteristics of melting ice slurries in compact plate heat exchangers, Int. Congr. Refrigeration, ICR0597, 16–23 August 2003, Washington, DC.

[8] Y. Yamagishi, H.T. Takeuchi, A.T. Pyatenko, N. Kayukawa, Characteristics of microencapsulated PCM slurry as a heat-transfer fluid, AIChE J. 45 (4) (1999) 696–707.

[9] J.J. Salamone, M. Newman, Heat transfer design characteristics: water suspensions of solids, Ind. Eng. Chem. 47 (2) (1955) 283–288.

[10] E. Stamatiou, M. Kawaji, Thermal and flow behavior of ice slurries in a vertical rectangular channel. Part I: Local distribution measurements in adiabatic flow, Int. J. Heat Mass Transfer, in press, doi:10.1016/j.ijheatmasstransfer.2005.03.020.

[11] E.N. Jensen, K.G. Christensen, T.M. Hansen, P. Schneider, M. Kauffeld, Pressure drop and heat transfer with ice slurry, in: Final Proceedings of the IIR-Gustav Lorentzen Conference on Natural Working Fluids at Purdue, Ray W. Herric Laboratories, West Lafayette, IN, 25–28 July 2000, pp. 572–580.

[12] E. Choi, Y.I. Cho, H.G. Lorsch, Forced convection heat transfer with phase-change-material slurries: turbulent flow in a circular tube, Int. J. Heat Mass Transfer 37 (2) (1994) 207–215.

[13] R.K. Shah, A.L. London, Laminar Flow Forced Convection in Ducts, A Source Book for Compact Heat Exchanger Analytical Data, Academic Press, New York, 1978, pp. 44–46.

[14] C.W. Snoek, J. Bellamy, Heat transfer measurements of ice slurry in tube flow, Exp. Heat Transfer, Fluid Mech. Therm. (1997) 1993–1997.

[15] B.D. Knodel, D.M. France, U.S. Choi, M.W. Wambsganss, Heat transfer in ice-water slurries, Appl. Therm. Eng. 20 (2000) 671–685.

[16] J.C. MaxwellA Treatise on Electricity and Magnetism, third ed., vol. 1, Dover, New York, 1954, pp. 440–441.

[17] E.J. Wasp, P.J. Kenny, R.L. Gandhi, Solid–liquid Flow Slurry Pipeline Transportation, Gulf Publishing Co., Houston, 1979.

[18] P.C. Augood, M. Newborough, D.J. Highgate, Thermal behaviour of phase-change slurries incorporating hydrated hydrophilic polymeric particles, Exp. Therm. Fluid Sci. 25 (2001) 457–468.

[19] D.G. Thomas, Transport characteristics of suspension: VIII. A note on the viscosity of Newtonian suspensions of uniform spherical particles, J. Colloid Sci. 20 (1965) 267–277.

[20] B. Metais, E.R.G. Eckert, Forced, mixed and free convection regimes, ASME J. Heat Transfer 86 (1964) 295–296.

[21] T. Kawanami, S. Fukusako, M. Yamada, Cold heat removal characteristics from slurry ice as a new phase change material, in: Natural Working Fluids '98, IIR-Gustav Lorentzen Conference: Proceedings of the Conference of Commission B2 with B1, E1 and E2, 1998, Oslo, Norway, pp. 146–156.

[22] T. Kawanami, S. Fukusako, M. Yamada, K. Itoh, Experiments on melting of slush ice in a horizontal cylindrical capsule, Int. J. Heat Mass Transfer 42 (15) (1999) 2981–2990.

[23] E. Stamatiou, Experimental Study of the Ice Slurry Thermal-Hydraulic Characteristics in Compact Plate Heat Exchangers, PhD Thesis, University of Toronto, Toronto, Ontario, Canada, 2003.

[24] W.M. Kays, M.E. Crawford, Convective Heat and Mass Transfer, third ed., McGraw-Hill Inc., New York, 1993, pp. 342–344.
[25] W. Nusselt, Der Wärmeaustausch zwischen wand und wasser im rohr, Forsch. Geb. Ingenieurwes. 2 (1931) 309.
[26] J.G. Knudsen, D.L. Katz, Fluid Mechanics and Heat Transfer, McGraw-Hill Book Company Inc, New York, 1958, pp. 400–403.
[27] J.P. Holman, Heat Transfer: Seventh Edition in SI Units, McGraw-Hill Book Company, New York, 1992.
[28] Y. Chin, M.S. Lakshminarasimhan, D.K. Hollingsworth, L.C. Witte, Convective heat transfer in vertical asymmetrically heated narrow channels, ASME J. Heat Transfer 124 (2002) 1019–1025.
[29] V. Gnielinski, New equations for heat and mass transfer for turbulent pipe and channel flow, Int. Chem. Eng. 16 (2) (1976) 359–368.
[30] V. Gnielinski, Forced convection ducts, in: E.U. Schlunder (Ed.), Heat Exchanger Design Handbook, Hemisphere, DC, 1983, pp. 2.5.1–2.5.3.
[31] K.G. Christensen, M. Kauffeld, Heat transfer measurements with ice slurry, Heat transfer issues in natural refrigerants, in: Proceedings of the Conference of Commission B1, with E1 & E2, Int. Inst. of Refrigeration, 6–7 November 1997, College Park, USA, pp. 161–176.
[32] R.P. Gupta, C.A. Fraser, Effect of a new friction reducing additive on Sunwell ice slurry characteristics, National Research Council of Canada, Institute of Mechanical Engineering, Low Temperature Laboratory, Report No. TR-LT-023, NRC, 1990, No. 32123.
[33] O. Sari, D. Vuarnoz, F. Meili, Visualization of ice slurries and ice slurry flows, in: Proceedings of the Second Workshop on Ice Slurries of IIF/IIR, Int. Inst. of Refrigeration, 2000, Paris, France.